SEMARAK ILMU PUBLISHING

CFD Letters

Journal homepage:
https://semarakilmu.com.my/journals/index.php/CFD_Letters/index
ISSN: 2180-1363

Numerical Prediction of Axisymmetric Jet Screech Tones in Supersonic Flows

Rithik R. Nambiar[1], Karthik Sankar K.[1], Manikandan M.[1,*], Balbir Singh[1], Manoj T. Nair[2]

[1] Department of Aeronautical and Automotive Engineering, Manipal Institute of Technology, Manipal Academy of Higher Education, Manipal, 576104, Karnataka, India
[2] Department of Aerospace Engineering, Indian Institute of Space Science and Technology, Thiruvananthapuram, 695547, Kerala, India

ARTICLE INFO

Article history:
Received 5 February 2025
Received in revised form 12 May 2025
Accepted 4 June 2025
Available online 20 August 2025

Keywords:
Computation Fluid Dynamics (CFD); Jet Screech Tones; Supersonic Jet; Acoustic Characteristics; Numerical Simulations; Turbulence modelling

ABSTRACT

This paper investigates into supersonic jet flows, focusing on the Mach number's crucial role in shaping jet screech tones. Employing meticulous computational fluid dynamics (CFD) techniques, the study reveals the profound influence of Mach numbers on the near-field screech tones from nozzles. The research explores pressure contours and frequency values across various Mach numbers, highlighting their intricate relationship and consequent impact on noise generation. Notably, screech tone intensity increases at lower frequencies and higher Mach numbers, validated through comparisons with experimental data. The methodology incorporates steady-state and transient-state analyses, utilizing Fast Fourier Transform plots for spectral analysis. The emergence of a significant sound pressure spike between 6000 Hz and 7000 Hz at Mach 1.2 signifies screech tones. The study observes a declining peak frequency with rising Mach numbers, alongside variations in shock wave strength and Mach cone width. Beyond advancing understanding, the paper establishes a foundation for future noise reduction strategies in jet engine design, promising implications for minimizing noise pollution and enhancing supersonic aircraft efficiency.

1. Introduction

The design of both subsonic and supersonic aircraft, as well as rotorcraft, is significantly influenced by noise concerns. These concerns extend to the current operational fleet, which is increasingly governed by stringent noise regulations [1-3]. The immediate need for noise reduction in aviation has catalysed active research in the field of aeroacoustics. An illustrative example of this is the reduction of jet noise through the enhancement of the bypass ratio in turbofan engines is demonstrated by Woodward *et al.* [4]. The generation of undesired noise in aircraft is typically a result of nonlinear, unsteady, and turbulent flows. The inherent complexity of these flows necessitates pragmatic simplifications for effective analysis and resolution. Central to aeroacoustics is the prediction and analysis of noise radiation from unsteady flows. This process begins with

* *Corresponding author.*
E-mail address: manikandan.m@manipal.edu

https://doi.org/10.37934/cfdl.18.4.3453

categorizing the issues based on the primary mechanisms of sound generation. To address the varied challenges in aeroacoustics, computational methods are being developed and refined. These methods address a spectrum of aeroacoustic issues, classified according to the physical processes responsible for sound radiation. This spectrum encompasses linear challenges involving radiation, refraction, and scattering in known base flows or around solid bodies, extending to the complex dynamics of sound generation by turbulence.

Computational Aeroacoustics (CAA), a vital component of aerospace engineering, combines aeroacoustics with computational fluid dynamics (CFD) to investigate sound generation and propagation in various aeroacoustic scenarios [5]. These contexts encompass air vehicles [6-8], wind turbines [9-12], high-speed trains [13-16], and automobiles [17-19]. The accurate prediction of aerodynamics and aeroacoustics through numerical methods is essential for modern sound design and optimization. Therefore, it requires thorough benchmarking of computational techniques supported by comprehensive acoustic data. In both commercial and military aviation, aeroacoustics plays a pivotal role, particularly in managing engine noise for operational considerations and certification compliance [20]. A central focus of aeroacoustics research is the study of jet noise, which examines turbulent eddies [21-23] and high-velocity jets [24-26], including turbulent mixing noise [27-29], broadband shock-associated noise [30,31], and screech tones [32-34].

Supersonic jets, especially those with shocks, often produce distinct, intense acoustic tones that indicate an aeroacoustic resonance loop within the flow. This noise comprises three distinct components: turbulent mixing noise, broadband shock-associated noise, and screech tones [35]. Turbulent mixing noise emerges from large-scale turbulent structures downstream, resembling Mach waves. Broadband shock-associated noise and screech tones occur when the jet's expansion is incomplete due to either over-expansion or under-expansion, leading to shock cells at the nozzle exit and additional noise components distinct from Mach waves. Broadband noise is referred to as broadband shock-associated noise, while the tonal noise is known as screech tones. Notably, screech tones primarily propagate upstream or in the opposite direction of the jet flow. A comprehensive study by Seiner [36] offers valuable insights into these three components of supersonic jet noise.

Screech, a unique aeroacoustic resonance in shock-containing supersonic jets, differs from other resonance phenomena as it does not involve interactions with downstream obstacles but rather originates entirely within the flow [25]. Screech tones, resulting from axisymmetric oscillations at low supersonic Mach numbers, stem from a feedback loop driven by jet flow instabilities and a quasiperiodic shock cell structure within the jet plume. Shock-containing supersonic jets frequently exhibit high-intensity, discrete-frequency acoustic tones, indicative of an aeroacoustic resonance loop established within the flow.

Recent studies have shown consistency between average speed profiles, shock distribution in shock cell jets, and experimental values. The interaction between stable and unstable waves near the nozzle lip across multiple shock cells generates acoustic radiation, completing the feedback loop. CAA utilizes numerical methods like Reynolds average Navier-Stokes (RANS) to predict broadband shock-associated noise (BBSAN), overcoming limitations of empirical models. RANS, a numerical method for turbulent flow, requires geometry and operating conditions, dividing flow values into measured and variable components. Its complexity necessitates mathematical calculations and special operators to simplify non-linear equations, providing insight into flow behaviour in complex systems. This modelling approach, while complex, offers flexibility for specific situations, contributing significantly to understanding and resolving aeroacoustic phenomena.

This paper aims to determine the jet shear layer in both steady and transient states and predict screech tones in under-expanded supersonic jets at various Mach numbers, using different microphone placements at the nozzle lip.

The literature reviewed encompasses seminal studies on screech tones in supersonic jets, spanning from early observations by Powell [37-39] to recent advancements by Miller *et al.* [40]. Initial discoveries by Powell highlighted the transition of noise into distinctive "whistling" screech tones upon surpassing critical pressure ratios in jets. Subsequent research by Richards [41,42] and Sperry et al. [43] expanded understanding, with investigations into shock wave interactions and nozzle designs impacting acoustical performance.

Further studies by various researchers, including Sarohia [44,45], Seiner *et al.* [46], Tam [47], and Panda and Seasholtz [48], investigated into the complexities of screech tone generation mechanisms, boundary layer transitions, and shock-associated noise phenomena. Computational methods, advocated by Thies and Tam [49] and Kurbatskii *et al.* [50,51], facilitated deeper insights into flow dynamics and acoustics, enabling precise simulations of screech tones and shock wave interactions.

Experimental studies by Ramani et al. [52], Munday et al. [53], and Lee [35] explored noise reduction techniques, flow structures, and numerical methods for screech tone prediction and suppression. Notably, investigations by Ye *et al.* [54] and Li *et al.* [55] highlighted the impact of nozzle geometries and simulation schemes on screech noise characteristics.

The reviewed literature underscores the intricate relationship between jet flow dynamics and acoustics, with significant advancements in understanding screech tone phenomena and noise reduction strategies. The present work aims to contribute to this body of knowledge by utilizing Computational Aeroacoustics (CAA) to model screech tone noise in axisymmetric supersonic jets. Employing a K-epsilon (k-ε) turbulence model and Direct CAA, the study analyses screech tone frequencies at various Mach numbers (M = 1.2, M = 1.5, M = 1.8) and assesses the influence of nozzle lip thickness on sound pressure levels. The research builds upon previous findings and methodologies, aiming to enhance understanding and mitigation of screech tones in supersonic jet propulsion systems.

2. Methodology

This research aims to detect screech tones in a supersonic free-flow jet at Mach Numbers 1.2, 1.5, and 1.8, and to assess the outcomes comparatively. The process involves examining an axisymmetric free jet under steady-state, low supersonic conditions. Subsequently, the gathered data is adjusted for transient flow analysis using the Realizable unsteady k-ε model. The Fast Fourier Transform (FFT) output is then subjected to spectral analysis to pinpoint the screech tones. The simulations were executed using ANSYS® Fluent, followed by data post-processing in CFD-Post.

2.1 Problem Description

This study investigates the performance of an axisymmetric jet at Mach numbers 1.2, 1.5, and 1.8, using a 0.0254 m diameter round nozzle with a wall-lip thickness of 0.0159 m. It focuses on detecting screech tones using microphones positioned at 0.0163 m and 0.0226 m from the wall lip. The simulation treats the nozzle exit as the inlet, without considering the internal nozzle geometry. Figure 1 presents the line diagram of the geometry, with its dimensions and mesh parameters detailed in Table 1.

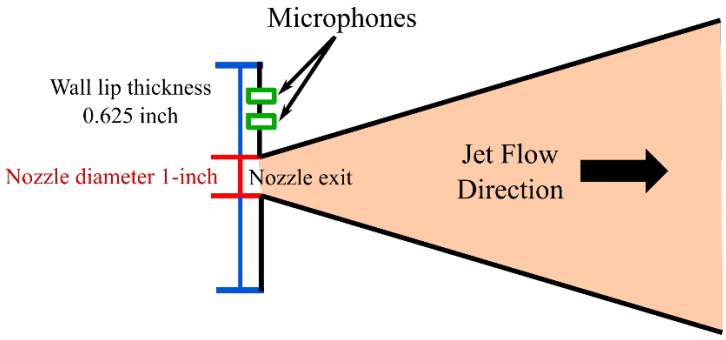

Fig. 1. Line diagram of the nozzle geometry

Table 1
Geometry and Mesh Parameters

Parameters	Values
Round jet inlet diameter(m)	0.0254
Wall lip thickness	0.0159
Far-field radius(m)	25.4
Nodes	1466904
Elements	1496645
Growth Rate	1.2
Quadrilateral mesh size	1e-4
Triangular mesh size	1.5

2.2 Boundaries in the simulation setup

The nomenclature of boundaries is mentioned as it represents. The Figure 2 depicts the named boundaries used in the simulation setup.

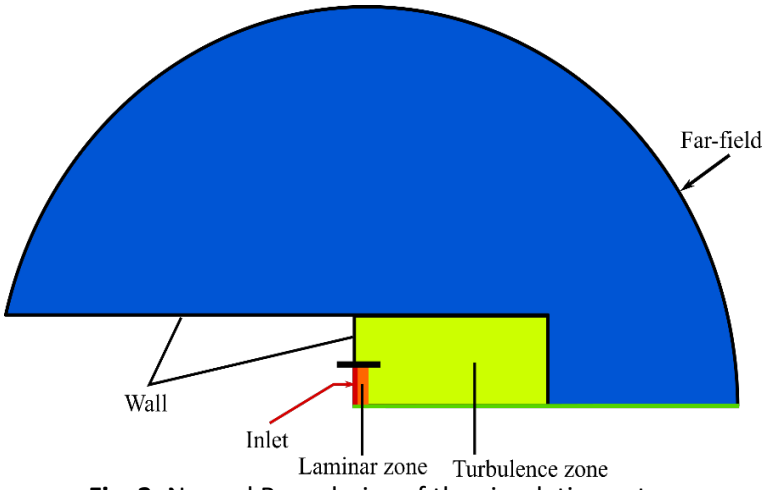

Fig. 2. Named Boundaries of the simulation setup

The far-field is modelled to simulate an open environment where jet noise can propagate freely without interference. The domain is extended approximately 500 acoustic wavelengths to ensure the acoustic waves like screech tones are naturally dissipated before reaching the boundary which prevents artificial reflections.

2.3 Mesh Geometry

The far-field region employs a 1.5 m triangular mesh, while the turbulence region, jet plume, and laminar zone utilize a finer 0.0001 m quadrilateral mesh. An enlarged view of the turbulent zone is shown in Figure 3. This finer mesh resolution observed in Figure 4 facilitates accurate capturing of phenomena such as jet shear layer excitations at the nozzle tip, shear layer instability wave generation, shock cell structure formation in the nozzle core, and the near-field propagation of screech acoustic waves.

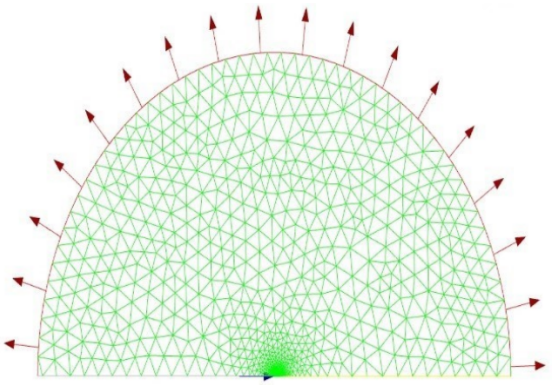

Fig. 3. Panned out image of meshed geometry

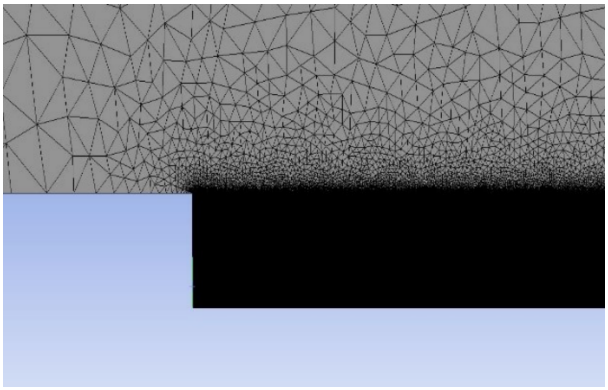

Fig. 4. Enlarged view of turbulent zone

2.4 Mesh Independent study

The simulation model is based on a hybrid quad-tri mesh. The behaviour of the jet plume in the near field up to about 20 nozzle diameters downstream is observed using structured quad cells. Triangular cells are used in the far field. A cell size of that order is needed to satisfactorily capture the excitations of the jet shear layer at the nozzle lip, the time-evolution of its instability waves, the structure of its shock cells in the core, and also the nearfield propagation of screech acoustic waves. The number of elements was varied from 1285 to 3828246 in order to check mesh independence as observed in Figure 5. It is observed that as the count of number of elements raises over 1496645, then the exit Mach number varying against number of elements was nearly approaching to zero. (slope is approximately zero). Consequently, a grid with 1496645 elements was deemed suitable for the investigation.

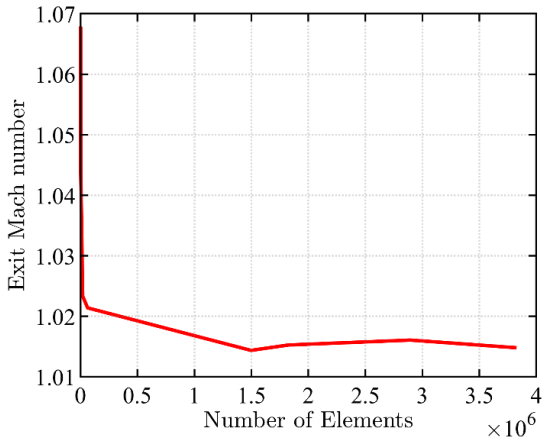

Fig. 5. Mesh Independence study plot

2.5 Model Setup

The model setup begins with two primary steps: verifying the mesh quality for accuracy and scaling it to meters for analysis. The study utilizes a two-dimensional steady-state axisymmetric model with a pressure-based solver. The structured mesh facilitates the use of the higher-order QUICK discretization method in CFD, enhancing resolution for parameters like density, energy, and momentum.

For turbulent jet flow prediction, the realizable k-ε viscous model, with constants adjusted following Tam and Thies [49], is employed. This model is known for its efficiency and reliability in complex scenarios. Near Wall Treatment employs the Standard Wall Function, and Table 2 lists the modified model constants.

Table 2
Realisable k- ε Model constants

Model Constants	Values
k- ε model with C2 module	2.02
Turbulent Prandtl Number (TKE)	0.324
Turbulent Prandtl Number (TDR)	0.377
Energy Prandtl Number	0.422

The ANSYS FLUENT® solver, utilizing the Finite Volume method (FVM), is employed to solve the primary governing equations for mass, momentum, and energy. These equations, under steady-state conditions, are addressed with double precision accuracy to mitigate the impact of typical round-off errors. A second-order upwind scheme is implemented for modelling fluid flow, turbulent kinetic energy, and other convective variables [56]. The fundamental governing equations for fluid flow are outlined below.

2.5.1 Continuity Equation (Conservation of Mass)

"The rate of change of mass of a fluid element is equal to the net rate of mass flow across its control volume." The two-dimensional continuity equation for compressible jet flow is expressed as:

$$\frac{\partial(\rho u)}{\partial x}+\frac{\partial(\rho v)}{\partial y}=0 \tag{1}$$

Where, u and v are the velocity components along the x and y directions, respectively, and ρ is the air density.

2.5.2 Momentum Equation

The momentum equation, derived from Newton's second law of motion, asserts that the sum of all forces acting on a fluid element is equal to the product of the mass of the fluid element and its acceleration. In the direction of jet flow x −direction, the momentum equation is:

$$\frac{\partial(\rho u^2)}{\partial x}+\frac{\partial(\rho uv)}{\partial y}=-\frac{\partial p}{\partial x}+\rho V_f \tag{2}$$

Similarly, in the direction perpendicular to jet flow $((y) - direction)$, the momentum equation is:

$$\frac{\partial(\rho uv)}{\partial x} + \frac{\partial(\rho v^2)}{\partial y} = -\frac{\partial p}{\partial y} + \rho V_f \tag{3}$$

Where $\tau_{xy}\ and \tau_{yy}$ denote shear stresses in the $x\ and\ y$ directions, respectively.$\sigma_{xx}\ and\ \sigma_{yy}$ are normal stresses acting in the $x\ and\ y$ directions, respectively. $F_x\ and\ F_y$ represent body forces per unit mass along the $x\ and\ y$ directions.

2.5.3 Energy Equation

The energy equation, based on the first law of thermodynamics, states that the rate of change of energy inside a fluid element is equal to the net rate of heat transfer and work done on the fluid element. Mathematically, this is expressed as:

$$\rho\left(\frac{\partial e}{\partial t} + u\frac{\partial e}{\partial x} + v\frac{\partial e}{\partial y}\right) = -\frac{\partial(pu)}{\partial x} - \frac{\partial(pv)}{\partial y} + \frac{\partial}{\partial x}\left(k\frac{\partial T}{\partial x}\right) + \frac{\partial}{\partial y}\left(k\frac{\partial T}{\partial y}\right) + q \tag{4}$$

Where q, e, k, $and\ p$ are the source term per unit mass, internal energy, thermal conductivity, and pressure, respectively.

2.5.4 Turbulence Model

The Realizable $(k - \varepsilon)$ turbulence model is applied to capture turbulence effects. The transport equations for k (turbulent kinetic energy)$and\ \varepsilon$ (turbulent dissipation) in this model are:

$$\frac{\partial}{\partial x_j}(\rho k u_j) = P_k - \beta^*\rho\varepsilon k + \frac{\partial}{\partial x_j}\left[\left(\mu + \frac{\mu_t}{\sigma_k}\right)\frac{\partial k}{\partial x_j}\right] \tag{5}$$

$$\frac{\partial}{\partial x_j}(\rho\varepsilon u_j) = P_\varepsilon - \beta\rho\varepsilon^2 + \frac{\partial}{\partial x_j}\left[\left(\mu + \frac{\mu_t}{\sigma_\varepsilon}\right)\frac{\partial \varepsilon}{\partial x_j}\right] \tag{6}$$

Where $P_k\ and\ P_\varepsilon$ are the turbulent production terms, μ_t is the turbulent viscosity, $\sigma_k\ and\ \sigma_\varepsilon$ are the turbulent Prandtl numbers, and $\beta\ and\ \beta^*$ are constants. The model constant C_1 is evaluated as:

$$C_1 = \max\left(0.43, \frac{S}{S_{ij}}\right) \tag{7}$$

Where $S\ and\ S_{ij}$ are the strain tensor and mean strain rate, respectively.

2.5.5 Modelling Turbulent Viscosity

The turbulent viscosity is an additional viscosity term used in turbulence models to account for the effect of turbulence on momentum transfer.

$$\mu_t = C_\mu\frac{k^2}{\varepsilon} \tag{8}$$

where C_μ is the model constant. The constants $A\ and\ s$ are defined as:

$$A = 4.04, \quad s = \cos(\theta), \quad \theta = \arccos\left(\frac{S_{ij}S_{ij}}{S^2}\right) \tag{9}$$

Model constants are $C_1 = 1.44, C_2 = 1.9, C_\mu = 0.09,$ and $C_\varepsilon = 1.3$.

2.6 Cell zone and Boundary conditions

In this configuration, compressed air at its optimal state serves as the working medium. The fluid's viscosity is determined using Sutherland's three coefficient method, assuming the density of an ideal gas. To amplify instability waves in the mixing layer, the nozzle is divided into a smaller laminar section and a larger turbulent section, achieved by setting the operating pressure to 0 Pa and applying isentropic relations for the fully expanded jet at specific Mach numbers. Turbulent intensity at the nozzle exit is low, at 0.1, and the jet is considered cold, with a total temperature equal to the ambient static pressure. Comprehensive boundary conditions used and the simulation setup is listed in the subsequent Tables 3-6.

Table 3
Fluid Properties

Parameters	Value/Settings
Density Calculation Method	Ideal Gas Law
Specific Heat (Cp) (J/kg-K)	1006.43
Thermal Conductivity (W/m-K)	0.0242
Viscosity model	Sutherland's Law
Sutherland Constant (K)	110.4
Reference Viscosity(kg/m-s)	1.716e-5
Reference Temperature (K)	273.15

Table 4
Inlet boundary conditions

Parameters	Value/Settings
Boundary Type	Pressure Inlet
Initial Gauge Pressure (Pa)	127360
Turbulent intensity (%)	0.1
Hydraulic Diameter (m)	0.0254
Total Temperature (K)	300

Table 5
Far-field boundary conditions

Parameters	Value/Settings
Boundary Type	Pressure Outlet
Gauge Pressure (Pa)	100000
Backflow Turbulent intensity (%)	1
Backflow Turbulent Viscosity Ratio	2
Backflow Total Temperature (K)	300

Table 6
Wall boundary conditions

Parameters	Value/Settings
Shear Condition	Specified Shear
X-component Shear (Pa)	0
Y-component Shear (Pa)	0
Roughness constant	0.5
Heat Flux (W/m^2)	0

Slip walls are used to model the boundaries in this study, as screech tones from free jet flows are minimally affected by them. Details of the boundary conditions are provided in Figure 5. This simulation setup enables a detailed analysis of the jet flow screech tones, informing improvements in supersonic jet efficiency and design optimization. The aerospace industry, including military jets, supersonic transport aircraft, and rocket engines, considers the analysis of supersonic jet flows vital for the development and advancement of various aircraft and spacecraft.

The governing equations implemented at these boundaries follow the standard Navier- Stokes formulation. At the pressure inlet boundary, the total pressure condition is enforced using:

$$\frac{P}{P_t} = \left(1 + \frac{\gamma-1}{2} M^2\right)^{\frac{-\gamma}{\gamma-1}} \tag{10}$$

Where γ is the ratio of specific heats (1.4 for air) and M is the Mach Number.

At the slip wall boundaries, the impermeability condition n.v = 0 is applied, where n is the unit normal vector to the wall and v is the velocity vector. This ensures zero mass flux across the wall while allowing tangential flow without friction.

To calculate the total gauge pressure at different Mach numbers, a static pressure of 1e5 Pa was employed, and the isentropic relation mentioned above in equation 10 was used to ascertain the stagnation pressure. The values derived from equation 10 for different Mach numbers are listed in the following Table 7.

Table 7
Gauge Total pressure for corresponding Mach Numbers

Mach Number	P/P_t	Pressure (Pa)
1.2	0.4124	242497
1.5	0.2724	367107
1.8	0.1740	574713

2.7 Solution Methods, Controls and Initialisation

The Pressure-Velocity coupling scheme is favoured in solution methods for steady flows due to its robustness and efficiency, optimizing performance. However, transient flows with large time steps necessitate a coupled algorithm. In gradient evaluations, the Green-Gauss node-based scheme proves superior. Employing QUICK discretization for density, momentum, and energy enhances the efficacy of a pressure-based solver, as discussed earlier. Solver settings are summarised and consolidated in Table 8.

Table 8
Solver settings

Parameters	Value/Settings
Time formulation	Steady & Transient
Pressure Velocity Coupling	Coupled
Gradient Discretization	Green-Gauss Node Based
Pressure Discretization	Standard
Momentum Discretization	QUICK
Energy Discretization	QUICK
Transient Formulation	Second-Order Implicit

The Courant Number, a critical dimensionless value in transient simulations, helps determine the appropriate time step relative to mesh size and flow velocity. For this test case, it is set at 50. Initialization data for the flow are detailed in Table 9.

Table 9
Data for flow initialization

Initialization Parameters	Value
Gauge pressure (Pa)	10^5
Axial velocity (m/s)	0
Radial velocity (m/s)	0
Turbulent kinetic energy (m^2/s^2)	0.1
Turbulent dissipation rate (m^2/s^3)	6
Temperature (K)	300

The steady-state analysis, conducted over 200 iterations, uses CFD-Post for post-processing to visualize the shock structure and Mach number contour. Optimizing this analysis requires scrutinizing the steady-state data. For transient analysis, the formulation is shifted to transient with a Second-order Implicit method. To improve the transient pressure-based coupled solver, the Courant number is raised to 1e-15, removing Implicit Relaxation factors. Explicit and Under-Relaxation factors are set at 1. Table 10 details the necessary parameters for transient flow iterations. Post-processing is conducted in CFD-Post after 20,000 iterations.

Table 10
Transient flow iteration parameters

Parameters	Value
Time stepping method	Fixed
Time step size	5e-06
Number of time steps	2000
Maximum iterations per time step	10

2.8 Acoustic Post-processing

The Ffowcs-Williams and Hawkings (FW-H) Acoustic model is employed [57-59], with microphones positioned along the jet's wall lip for FFT spectral analysis. The procedure for computing sound using the FW-H acoustics model in ANSYS® FLUENT consists largely of two steps. In the first step, a time-accurate flow solution is generated from which time histories of the relevant variables (e.g., pressure, velocity, and density) on the selected source surfaces are obtained. In the second step, sound pressure signals at the user-specified receiver locations are computed using the source data collected during the first step. The spectral plot uses FFT, showing frequency on the x-axis and Sound Pressure Level (SPL) on the y-axis. To maintain the plot within a specific range, values outside

this range are clipped. After configuring the solver with these settings, the model undergoes simulation. The output is then analysed to understand the screech tone behaviour, leading to observations, analysis, and conclusions drawn from the output data.

3. Results and Discussion

3.1 Steady-state analysis

A steady-state analysis was performed to calibrate a model for transient-state simulations of the jet-shear layer. Velocity contours at Mach numbers 1.2, 1.5, and 1.8 are computed and illustrated in Figures 6a, 6b, and 6c, respectively. These figures reveal the formation of shock-cell structures from the nozzle exit in each case.

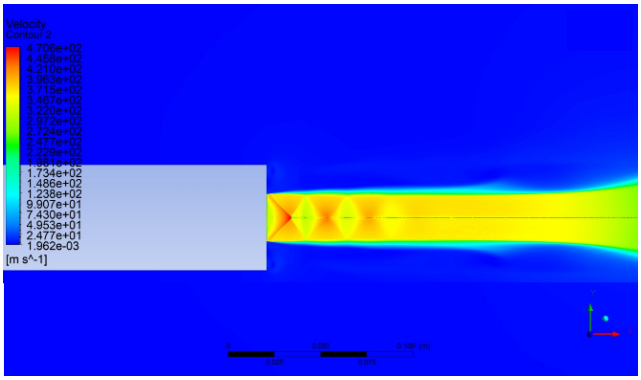

Fig. 6a. Shock-cell formation in steady-state simulation at Mach Number=1.2

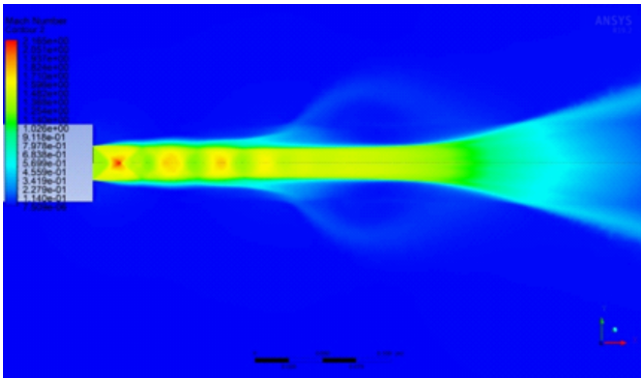

Fig. 6b. Shock-cell formation in steady-state simulation at Mach Number=1.5

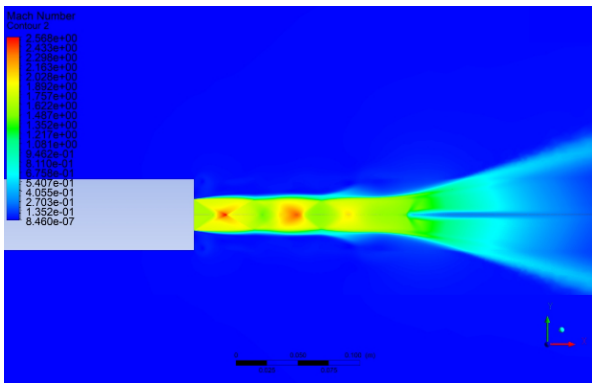

Fig. 6c. Shock-cell formation in steady-state simulation at Mach Number=1.8

In the steady state, simulations are based on the constant flow properties, such as velocity and pressure. Therefore, the dynamic and time-dependent phenomena, such as the formation and evolution of shock cells, will be damped or not fully represented. Transient simulations, on the other hand, allow the opportunity to explicitly show the time-varying conditions and can thus, for instance, provide a better view of phenomena such as shock cell formation.

3.2 Transient-state analysis

There is a notable difference in velocity contours between steady-state and transient-state simulations, with the shock-cell structure being less pronounced in steady-state. Transient

simulations provide a more efficient and approximate solution. The formation of shock structures in transient states is evident.

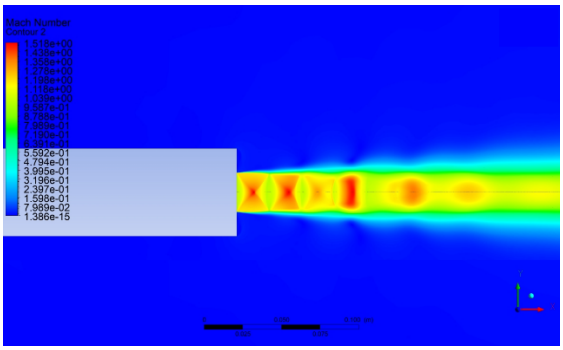

Fig. 7a. Shock-cell formation in transient-state simulation at Mach Number=1.2, showing well-defined diamond patterns with distinct boundaries between consecutive cells that serve as powerful acoustic sources.

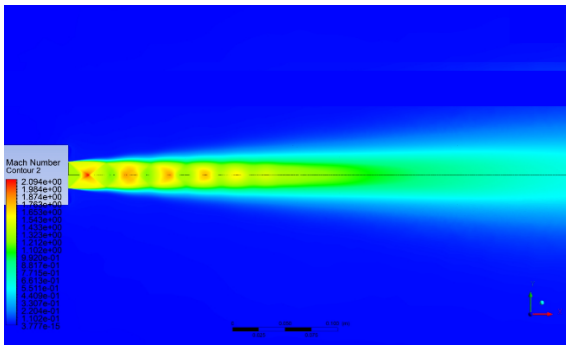

Fig. 7b. Shock-cell formation in transient-state simulation at Mach Number=1.5, displaying axially elongated cells with increased spacing and more diffuse intensity gradients compared to the Mach 1.2 case.

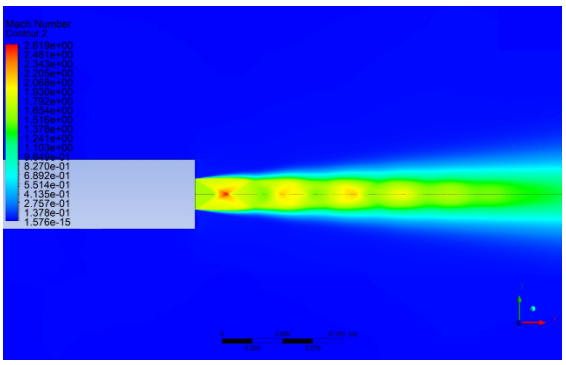

Fig. 7c. Shock-cell formation in transient-state simulation at Mach Number=1.8, demonstrating further elongation of shock cells with less distinct boundaries and increased lateral expansion of the jet plume.

Figure 7a reveals the complex shock-cell structures at Mach 1.2. The shock structures are characterized by well-defined diamond patterns with distinct boundaries between consecutive cells. The shock diamonds thus formed are the characteristic features of the moderately under-expanded jets, where the static pressure at the exit of the nozzle exceeds the ambient pressure of the surroundings. The initial shock cells demonstrate particularly high intensity gradients that function as powerful acoustic sources with the flow field. These high-gradient regions create necessary condition for strong interaction between vortical structures in the shear layer and the shock waves, a critical mechanism in screech generation.

When the Mach number increases to 1.5 as depicted in the Figure 7b, significant morphological transformations can be observed in the shock cell structure. The observations are that the cells are axially elongated with increased spacing between the successive shock waves which is in accordance with the gas dynamics theory. The axial elongation follows the relationship first established by Pack [62]

$$L \propto D\sqrt{(M^2 - 1)} \tag{11}$$

Where L is the shock-cell length, D is the nozzle diameter, and M is the Mach number. This relationship between shock-cell spacing and Mach number is a direct consequence of the gas dynamics governing supersonic flows. As the Mach number increases, the pressure differential that drives the formation of shock cells creates expansion waves that travel at greater distances before reflecting from the jet boundary, resulting in longer shock cells. This physical mechanism explains why the spacing increases proportionally with $\sqrt{(M^2-1)}$. The intensity gradient within each cell appears more diffuse compared to the Mach 1.2 simulation setup. The feedback mechanism must traverse greater distances between the nozzle lip and the shock structures which correlates with the observed reduction in screech frequency.

Further evolution of shock-cells structure can be observed in the Mach 1.8 simulation setup as shown in Figure 7c. The shock-cells expand farther downstream before dissipating, and the jet exhibits increased lateral expansion due to enhanced entrainment and mixing. Less distinction of the shock boundaries especially in the downstream regions which implies formation of a more complex three-dimensional flow structures with increased turbulent mixing. Mach cone width shows a proportional correlation with Mach number which depicts a broader jet plume with more gradual pressure gradients across shock interfaces.

These progressive alterations in shock-cell configuration across the Mach number range demonstrate a fundamental relationship between flow structure and acoustic characteristics. Observing our spectral analysis, the increase in shock-cell spacing with Mach number throws light into the physical explanation demonstrating inverse correlation between Mach number and screech frequency. As the shock cells become larger, the time for the disturbance to travel downstream along the shock structure and the resulting acoustic wave to propagate upstream to reach nozzle lip increases, thereby decreasing the frequency of the feedback loop.

At lower Mach numbers (M=1.2), the well-defined shock cells with sharp gradients aids in the strong coupling between flow instabilities and acoustic feedback. As Mach number increases, this coupling mechanism evolves due to changes in shock strength, spacing and interaction with surrounding shear layer.

3.3 Validation Study

The validation protocol adhered to the framework delineated by Kurbatskii [50] in their study on numerical methodologies. This framework was specifically chosen due to its comprehensive approach to validating computational aeroacoustics simulations and its established reliability in predicting screech tones in supersonic jets. The validation process entailed the strategic placement of dual microphones at the nozzle's edge to monitor and forecast the screech tone characteristics at a Mach number of 1.2.

The pivotal metric for this validation was the screech peak frequencies, which represents the most distinctive and measurable feature of the screech phenomenon. This metric was selected over alternatives such as overall sound pressure level or broadband noise characteristics because screech tones exhibit discrete frequencies that can be precisely identified and compared. Notwithstanding the simulation's susceptibility to variations as highlighted in Norum's [60] research on screech tones, the stability of the screech peak frequencies was notable, exhibiting slight deviations in their recorded values.

Figure 8 presents a comparison between computational analysis by Kurbatskii [50] and CFD simulations, shown as a dashed blue line and a solid red line. Both demonstrate similar oscillatory patterns with primary maxima near 6 kHz where empirical data surpassing 140 dB and CFD just below this threshold. This frequency corresponds to the axisymmetric mode(A-mode) of screech, which

typically predominates at lower supersonic Mach numbers in circular jets. The primary peak represents the fundamental frequency of the feedback loop mechanism where shear instabilities interact with the shock-cell structure to generate acoustic waves that propagate upstream. These waves trigger new instabilities at the nozzle lip, thus completing the self-sustaining resonance feedback loop.

Following this peak, both profiles decrease, showing a secondary maximum around 8 kHz before declining. The presence of the multiple spectral peaks suggests a complex acoustic field with mode switching behaviour or harmonic responses. The CFD simulation, despite its sensitivity, shows stable screech frequency peaks with minor variances and sound pressure level fluctuations due to mesh differences, turbulence constants, and environmental factors.

On quantitatively analysing the validation results, it can be inferred that the screech tones are predominantly confined to 6-7 kHz, with our model achieving a validation error of approximately 1% in predicting frequency.

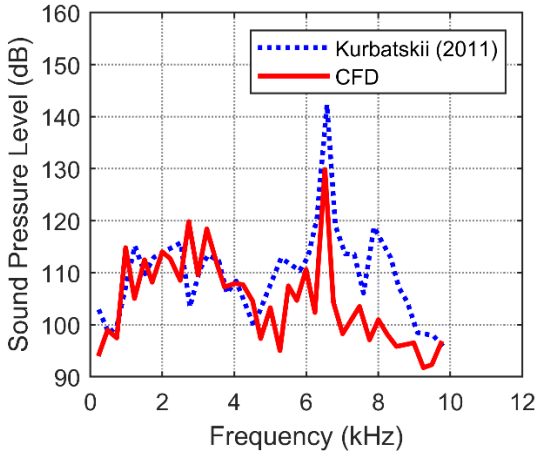

Fig. 8a. Numerical validation of screech tones from Mic 1 at Mach 1.2

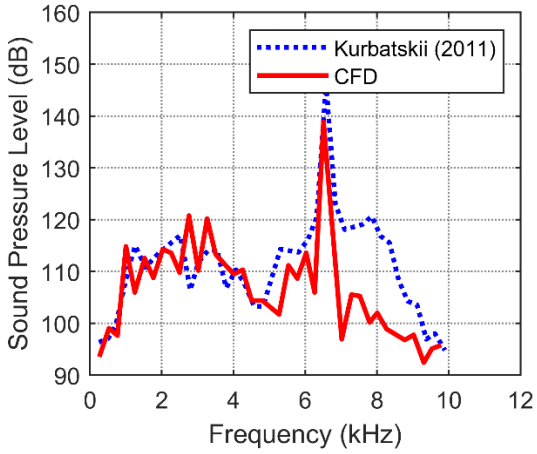

Fig. 8b. Numerical validation of screech tones from Mic 2 at Mach 1.2

However, our CFD model slightly underpredicts at 6kHz peak compared to the empirical measurements suggest the limitations imposed by the numerical model on the simulation. These underpredictions can be the consequence of the following listed below:

- Simplification and approximation in turbulence modelling, particularly in capturing the highly unsteady processes in the shear layer where vortical structures interact with shock waves.
- Inherent numerical dissipation in the discretization scheme can dampen the acoustic wave amplitudes.
- Limitation encountered in resolving the smallest scales of turbulence that contribute to the acoustic field.
- Potential differences in the exact geometry, far-field or flow conditions.

Despite the amplitude discrepancies, our simulation captures the primary physical mechanisms responsible for the generation of screech tones and the spectral peaks results are in close agreement with the validation results. This consistency across the studies adds confidence in the generated results.

To quantify the validation performance more precisely, the normalised root mean square error (NRMSE) between the predicted CFD data and the reference data across the entire frequency spectrum. The resulting NRMSE value of 8.4% indicates overall good agreement. The error contribution is due to the amplitude difference rather than the frequency shifts.

3.4 Sound Pressure Level (SPL) Analysis

The SPL versus Frequency graph demonstrates detected screech tones at various Mach numbers. FFT analyses from Microphone 1 and Microphone 2, placed on the nozzle lip, reveal screech tone modes at each Mach number, indicated by spikes in both plots. The most prominent sound pressure peak, consistent with Ponton and Seiner's (1992) findings, occurs between 6000-7000 Hz. Analysis in Figure 9a and Figure 9b for M = 1.5 shows a peak in the 4000-5000 Hz range, while Figure 10a and Figure 10b for M = 1.8 indicates a peak around 2000 Hz. This systematic shift in peak frequency in axisymmetric jets indicates a clear inverse relation between Mach number and screech frequency which was originally proposed by Powell [37] and can be expressed as which is expressed as

$$f \propto 1/\sqrt{(M^2-1)} \tag{12}$$

which aligns with the theoretical models of generation of screech tones based on spacing of shock-cells and acoustic feedback mechanism. The inverse relationship between screech frequency and Mach number is a direct consequence of the feedback loop mechanism that generates screech. Since the frequency of the screech tone is inversely proportional to the time required for disturbances to travel downstream through the shock structure and for the resulting acoustic waves to propagate upstream to the nozzle lip, the increase in shock-cell spacing at higher Mach numbers naturally leads to a decrease in screech frequency. This physical mechanism provides a fundamental explanation for the observed spectral shifts across different Mach regimes.

The observed frequency transition across the Mach number range demonstrates acoustic mode transitions in axisymmetric jets. At Mach 1.2, depicted in Figure 8a and Figure 8b, the dominant frequency ranging from 6000-7000Hz corresponds to the axisymmetric mode (A-mode), characterised by the toroidal vortex structure in the shear layer.

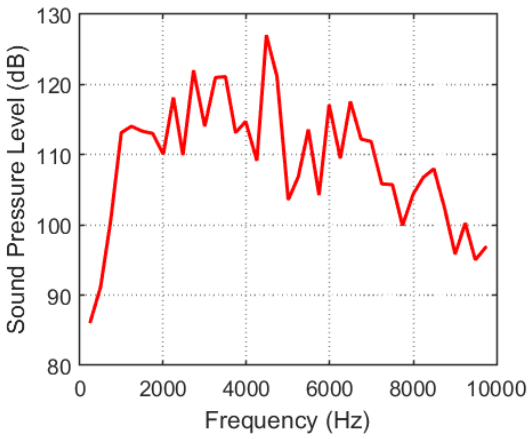

Fig. 9a. Spectral plot for Mach 1.5 for Mic 1

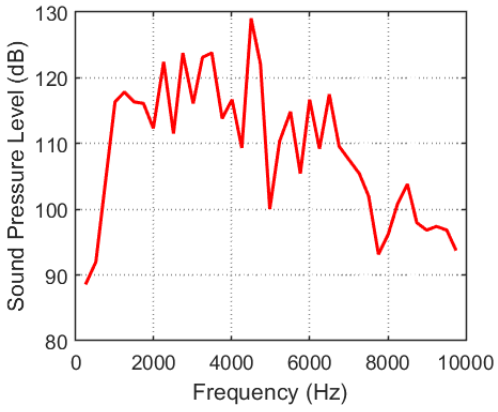

Fig. 9b. Spectral plot for Mach 1.5 from Mic 2

Inferring from Figure 9a and Figure 9b, for flow with Mach 1.5, there is a shift in peak frequency to a range 4000-5000Hz which demonstrates the transition to flapping mode (B-mode). These are characterised by sinuous, lateral oscillations of jet column.

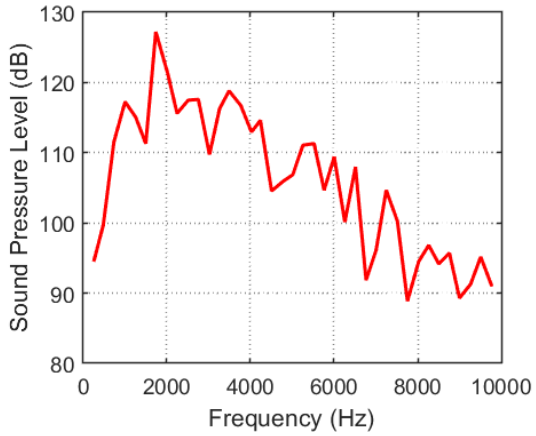

Fig. 10a. Spectral plot for Mach 1.8 from Mic 1

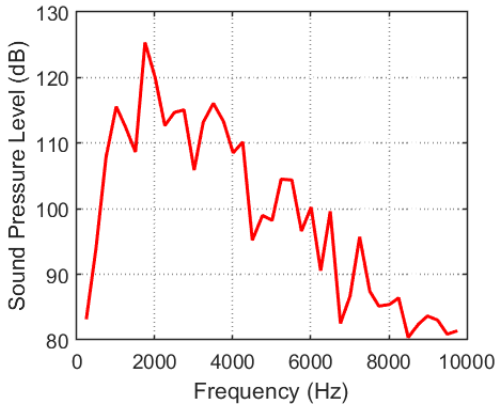

Fig. 10b. Spectral plot for Mach 1.8 from Mic 2

Evaluating for flow speed of Mach 1.8 from Figure 10a and Figure 10b, there is a sudden decrease in frequency which drops to approximately 2000Hz. This suggests the emergence of helical mode (C-mode) with complex three-dimensional oscillation patterns.

The consistent observation of these frequency transitions across both microphone positions confirms the robustness of the phenomenon. The inverse relationship between Mach number and screech frequency has significant implications for noise control strategies in supersonic propulsion systems. As the acoustic mode transition with increasing Mach number, both the frequency and directivity patterns of the noise deviate substantially. Noise reduction and mitigation approaches should account for the modal transitions, variation in frequency for effectively addressing the dominant screech tone characteristics.

The observed modal transitions correlate directly with the changes in shock-cell structure. The elongation of shock-cell with change in Mach number accounts for increase in wavelength of the instability waves. The consequence being reduction in frequency of resulting acoustic feedback loop. This direct connection between flow structure and acoustic behaviour emphasises on the need for understanding the fluid dynamics of the jet predicting and controlling acoustic characters.

4. Conclusions

This study is dedicated to predicting jet screech noise emitted by a supersonic jet nozzle, employing computational aeroacoustics simulations across various supersonic Mach numbers. This research is undertaken to fill the existing gap in formulating a formula for screech tone intensity and direction trying to improve through the comparison with the experimental data. The central point is to predict Mach number variation with respect to screech tone.

A realizable k-ε model has been purposely used for assuring the fidelity of the simulations. The model for optimization was well analysed for a steady state, calibrated by the transient state simulations for improvement of the modelling accuracy. This was through the use of a pressure-based solver. Following these simulations, comprehensive microphone data was methodically collected and then subsequently analysed.

It should be noted that further spectral analysis using FFT showed a spike at 6000-7000 Hz in sound pressure level at Mach 1.2, thus leaving no doubts about the presence of screech within the

supersonic flow. It was observed to be a relationship where Mach number increments along with a decrease in peak frequency pointed towards a narrowing of the Mach cone width and thinner shock waves.

Detailed analysis of the shock-cell structure across different Mach numbers revealed that the spacing between shock-cells increases with Mach number according to the established gas dynamics principles. This increased spacing directly correlates with the observed decrease in screech frequency, establishing the fundamental physical principle behind the Mach number-frequency relationship. The transition of acoustic modes demonstrates the complex evolution of flow-acoustic coupled with altering flow conditions.

The validation study against reference data interprets that the results show good agreement with the frequency predictions (within 1% error) and reasonable agreement in amplitude providing confidence in predictive capabilities of the computational methodology implemented for this research and its applicability to real-world supersonic jet noise scenarios.

This methodology significantly enhances our understanding and predictive capabilities regarding jet screech noise in supersonic jet nozzles. The findings have important implications for the design and optimisation of supersonic propulsion systems, particularly in applications where noise reduction is a critical concern. By understanding the relationship between Mach number, flow structure and acoustic characteristics, engineers can develop more effective strategies in curbing and mitigating screech noise from high-speed propulsion systems.

Future work should focus on extending this analysis to more complex nozzle geometries and investigating the effects of temperature and pressure ratios on screech characteristics. Additionally, active control strategies targeting specific acoustic modes could be explored as potential noise reduction approaches for next-generation supersonic aircraft.

Acknowledgement
We authors express our sincere gratitude to the Manipal Institute of Technology, a constituent engineering institute of Manipal Academy of Higher Education, an Institution of Eminence that supported and facilitated the authors in their pursuit of knowledge and the dissemination of scientific insights.

Author Contributions
Design Model and Computational Framework - Rithik R. Nambiar and Karthik Sankar K; Conceptualization - Rithik R. Nambiar, Karthik Sankar K, Manikandan M., Balbir Singh and Manoj T. Nair ; Methodology - Rithik R. Nambiar, Karthik Sankar K, Manoj T. Nair; Software - Rithik R Nambiar and Karthik Sankar K; Validation -Rithik R. Nambiar, Karthik Sankar K and Manikandan M.; Writing---Original Draft preparation - Rithik R. Nambiar and Manikandan M.; Writing---Review and Editing - Manikandan M. and Balbir Singh; Supervision - Manikandan M., Balbir Singh and Manoj T. Nair. All authors have read and agreed to the published version of the manuscript.

Funding
This research received no external funding.

Data Availability
Some or all data, models, or codes that support the findings of this study are available from the corresponding author (Manikandan M. and Balbir Singh) upon reasonable request.

Conflicts of Interest

The authors declare no conflict of interest.

References

[1] Claes, Benedicte A. "Aircraft noise regulation in the European Union: The hushkit problem." *Journal of Air Law & Commerce* 65 (1999): 329.

[2] Abeyratne, Ruwantissa. "Some recent developments in aviation and environmental protection regulation." *Envtl. Pol'y & L.* 32 (2002): 32.

[3] Leylekian, Laurent, Alexandra Covrig, and Alena Maximova. Aviation Noise Impact Management: Technologies, Regulations, and Societal Well-being in Europe. *Springer Nature*, 2022. https://doi.org/10.1007/978-3-030-91194-2

[4] Woodward, Richard P., Christopher E. Hughes, and Gary G. Podboy. "Fan noise reduction with increased bypass nozzle area." *Journal of aircraft* 43, no. 6 (2006): 1719-1725. https://doi.org/10.2514/1.19359

[5] Colonius, Tim, and Sanjiva K. Lele. "Computational aeroacoustics: progress on nonlinear problems of sound generation." *Progress in Aerospace sciences* 40, no. 6 (2004): 345-416. https://doi.org/10.1016/j.paerosci.2004.09.001

[6] Campos, Luís MBC. "On physical aeroacoustics with some implications for low-noise aircraft design and airport operations." *Aerospace* 2, no. 1 (2015): 17-90. https://doi.org/10.3390/aerospace2010017

[7] Petrosino, Francesco, Mattia Barbarino, and Martin Staggat. "Aeroacoustics assessment of an hybrid aircraft configuration with rear-mounted boundary layer ingested engine." *Applied Sciences* 11, no. 7 (2021): 2936. https://doi.org/10.3390/app11072936

[8] Thomas, Russell H., Yueping Guo, Ian Clark, and Jason June. "Propulsion airframe aeroacoustics and aircraft system noise flight research test: NASA overview." In *28th AIAA/CEAS Aeroacoustics 2022 Conference*, p. 2993. 2022. https://doi.org/10.2514/6.2022-2993

[9] Weber, Johannes, Stefan Becker, Christoph Scheit, Jens Grabinger, and Manfred Kaltenbacher. "Aeroacoustics of Darrieus wind turbine." *International Journal of Aeroacoustics* 14, no. 5-6 (2015): 883-902. https://doi.org/10.1260/1475-472X.14.5-6.883

[10] Benim, Ali Cemal, Michael Diederich, Fethi Gül, Pawel Oclon, and Jan Taler. "Computational and experimental investigation of the aerodynamics and aeroacoustics of a small wind turbine with quasi-3D optimization." *Energy conversion and management* 177 (2018): 143-149. https://doi.org/10.1016/j.enconman.2018.09.042

[11] Traylor, Caleb, Milo DiPaola, David J. Willis, and Murat Inalpolat. "A computational investigation of airfoil aeroacoustics for structural health monitoring of wind turbine blades." *Wind Energy* 23, no. 3 (2020): 795-809. https://doi.org/10.1002/we.2459

[12] Cheng, Zhi, Fue-Sang Lien, Eugene Yee, and Hang Meng. "A unified framework for aeroacoustics simulation of wind turbines." *Renewable Energy* 188 (2022): 299-319. https://doi.org/10.1016/j.renene.2022.01.120

[13] Zhu, Jianyue, Zhiwei Hu, and David J. Thompson. "Flow behaviour and aeroacoustic characteristics of a simplified high-speed train bogie." *Proceedings of the Institution of Mechanical Engineers, Part F: Journal of Rail and Rapid Transit* 230, no. 7 (2016): 1642-1658. https://doi.org/10.1177/0954409715605129

[14] Zhu, Chunli, Hassan Hemida, Dominic Flynn, Chris Baker, Xifeng Liang, and Dan Zhou. "Numerical simulation of the slipstream and aeroacoustic field around a high-speed train." *Proceedings of the Institution of Mechanical Engineers, Part F: Journal of Rail and Rapid Transit* 231, no. 6 (2017): 740-756. https://doi.org/10.1177/0954409716641150

[15] Minelli, G., H-D. Yao, N. Andersson, P. Höstmad, J. Forssén, and S. Krajnović. "An aeroacoustic study of the flow surrounding the front of a simplified ICE3 high-speed train model." *Applied Acoustics* 160 (2020): 107125. https://doi.org/10.1016/j.apacoust.2019.107125

[16] Liu, Hongkang, Siqi Zhou, Rongrong Chen, Zhuolun Li, Shishang Zhang, and Yatian Zhao. "Numerical study on the aeroacoustic performance of different diversion strategies in the pantograph area of high-speed trains at 400 km/h." *Applied Sciences* 12, no. 21 (2022): 10702. https://doi.org/10.3390/app122110702

[17] Oettle, Nicholas, and David Sims-Williams. "Automotive aeroacoustics: An overview." *Proceedings of the Institution of Mechanical Engineers, Part D: Journal of Automobile Engineering* 231, no. 9 (2017): 1177-1189. https://doi.org/10.1177/0954407017695147

[18] Citarella, Roberto, and Luigi Federico. "Advances in vibroacoustics and aeroacustics of aerospace and automotive systems." *Applied Sciences* 8, no. 3 (2018): 366. https://doi.org/10.3390/app8030366

[19] Zaareer, Moath N., Abdel-Hamid Ismail Mourad, Tariq Darabseh, Kassim Abdullah, and Mostafa SA ElSayed. "Aeroacoustics wind noise optimization for vehicle's side mirror base." *International Journal of Thermofluids* 18 (2023): 100332. https://doi.org/10.1016/j.ijft.2023.100332

[20] Bernardini, Giovanni, Francesco Centracchio, Massimo Gennaretti, Umberto Iemma, Claudio Pasquali, Caterina Poggi, Monica Rossetti, and Jacopo Serafini. "Numerical characterisation of the aeroacoustic signature of propeller arrays for distributed electric propulsion." *Applied Sciences* 10, no. 8 (2020): 2643. https://doi.org/10.3390/app10082643
[21] Wasala, Sahan H., Rupert C. Storey, Stuart E. Norris, and John E. Cater. "Aeroacoustic noise prediction for wind turbines using Large Eddy Simulation." *Journal of Wind Engineering and Industrial Aerodynamics* 145 (2015): 17-29. https://doi.org/10.1016/j.jweia.2015.05.011
[22] Gea-Aguilera, Fernando, James Gill, and Xin Zhang. "Synthetic turbulence methods for computational aeroacoustic simulations of leading edge noise." *Computers & Fluids* 157 (2017): 240-252. https://doi.org/10.1016/j.compfluid.2017.08.039
[23] Ahn, Myeonghwan, Mihai Mihaescu, Aatresh Karnam, and Ephraim Gutmark. "Large-eddy simulations of flow and aeroacoustics of twin square jets including turbulence tripping." *Physics of fluids* 35, no. 6 (2023). https://doi.org/10.1063/5.0147295
[24] Gubanov, D. A., V. I. Zapryagaev, N. P. Kiselev, and S. G. Kundasev. "Aeroacoustic interaction in high-velocity jet with a thin obstacle." In *AIP Conference Proceedings*, vol. 2027, no. 1. AIP Publishing, 2018. https://doi.org/10.1063/1.5065296
[25] Edgington-Mitchell, Daniel. "Aeroacoustic resonance and self-excitation in screeching and impinging supersonic jets–a review." *International Journal of Aeroacoustics* 18, no. 2-3 (2019): 118-188. https://doi.org/10.1177/1475472X19834521
[26] Chen, Song, Romain Gojon, and Mihai Mihaescu. "Flow and aeroacoustic attributes of highly-heated transitional rectangular supersonic jets." *Aerospace Science and Technology* 114 (2021): 106747. https://doi.org/10.1016/j.ast.2021.106747
[27] Bai, Baohong, Xiaodong Li, and Haixin Chen. "A Semi-empirical Prediction Method for the Fine Scale Turbulence Mixing Noise." In *25th AIAA/CEAS Aeroacoustics Conference*, p. 2757. 2019. https://doi.org/10.2514/6.2019-2757
[28] Patel, Trushant K., and Steven AE Miller. "Source of fine-scale turbulent mixing noise using the Navier–Stokes equations." *AIAA Journal* 59, no. 6 (2021): 2333-2338. https://doi.org/10.2514/1.J059647
[29] Mu, Guozhen, Qiongying Lyu, and Yiming Li. "An analysis of jet noise characteristics in the compressible turbulent mixing layer of a standard nozzle." *Machines* 10, no. 10 (2022): 826. https://doi.org/10.3390/machines10100826
[30] Gryazev, V., A. Kalyan, A. P. Markesteijn, and S. A. Karabasov. "Broadband shock-associated noise modelling for high-area-ratio under-expanded jets." *The Journal of the Acoustical Society of America* 150, no. 2 (2021): 1534-1547. https://doi.org/10.1121/10.0005976
[31] Nogueira, Petrônio A., and Daniel M. Edgington-Mitchell. "Study of Broadband Shock-Associated Noise using the Parabolised Floquet Equations." In *28th AIAA/CEAS Aeroacoustics 2022 Conference*, p. 3063. 2022. https://doi.org/10.2514/6.2022-3063
[32] Gojon, Romain, and Christophe Bogey. "Numerical study of the flow and the near acoustic fields of an underexpanded round free jet generating two screech tones." *International Journal of Aeroacoustics* 16, no. 7-8 (2017): 603-625. https://doi.org/10.1177/1475472X17727606
[33] Morata, David, and Dimitri Papamoschou. "Effect of nozzle geometry on the space-time emission of screech tones." In *AIAA AVIATION 2021 FORUM*, p. 2306. 2021. https://doi.org/10.2514/6.2021-2306
[34] Jeun, Jinah, Aatresh Karnam, Gao Jun Wu, Sanjiva K. Lele, Florian Baier, and Ephraim J. Gutmark. "Aeroacoustics of twin rectangular jets including screech: large-eddy simulations with experimental validation." *AIAA Journal* 60, no. 11 (2022): 6340-6360. https://doi.org/10.2514/1.J060895
[35] Lee, Incheol, and Duck Joo Lee. "Investigation on the Source Locations of Axisymmetric Screech Tones Utilizing Data from Numerical Simulation." *Journal of Theoretical and Computational Acoustics* 27, no. 04 (2019): 1850058. https://doi.org/10.1142/S2591728518500585
[36] Seiner, J. "Advances in high speed jet aeroacoustics." In *9th Aeroacoustics conference*, p. 2275. 1984. https://doi.org/10.2514/6.1984-2275
[37] Powell, Alan. "The noise of choked jets." *The Journal of the Acoustical Society of America* 25, no. 3 (1953): 385-389. https://doi.org/10.1121/1.1907052
[38] Powell, Alan. "On the mechanism of choked jet noise." *Proceedings of the Physical Society. Section B* 66, no. 12 (1953): 1039. https://doi.org/10.1088/0370-1301/66/12/306
[39] Powell, Alan. "The reduction of choked jet noise." *Proceedings of the Physical Society. Section B* 67, no. 4 (1954): 313. https://doi.org/10.1088/0370-1301/67/4/306
[40] Miller, Kyle, David Morata, and Dimitri Papamoschou. "Effect of Nozzle Geometry on Near-Field Modal Content of a Screeching Jet." In *AIAA SCITECH 2023 Forum*, p. 0024. 2023. https://doi.org/10.2514/6.2023-0024

[41] Richards, E. J. "Research on aerodynamic noise from jets and associated problems." *The Aeronautical Journal* 57, no. 509 (1953): 318-342. https://doi.org/10.1017/S0368393100125131
[42] Richards, E. J. "On the noise from supersonic jets." *The Aeronautical Journal* 61, no. 553 (1957): 43-45. https://doi.org/10.1017/S0368393100130548
[43] Sperry, W. C., and Margaret Emmitt. *Fundamental Study of Jet Noise Generation and Suppression*. Vol. 1. Propulsion Laboratory, Wright Air Development Division, Air Research and Development Command, United States Air Force, 1960.
[44] Sarohia, V. "Effect of flight on jet noise from supersonic underexpanded flows." In *4th Aeroacoustics Conference*, p. 1328. 1977. https://doi.org/10.2514/6.1977-1328
[45] Sarohia, V. "Some flight simulation experiments on jet noise from supersonic underexpanded flows." *AIAA Journal* 16, no. 7 (1978): 710-716. https://doi.org/10.2514/3.60958
[46] Seiner, John M., Thomas D. Norum, and Lucio Maestrello. "Effects of nozzle design on the noise from supersonic jets." *Supersonic Cruise Res. 1979, Pt. 1* (1980).
[47] Tam, Christopher KW. "Supersonic jet noise." *Annual review of fluid mechanics* 27, no. 1 (1995): 17-43. https://doi.org/10.1146/annurev.fl.27.010195.000313
[48] Panda, Jayanta, and Richard G. Seasholtz. "Screech noise generation from supersonic underexpanded jets investigated." *Research and Technology 1999* (2000).
[49] Thies, Andrew T., and Christopher KW Tam. "Computation of turbulent axisymmetric and nonaxisymmetric jet flows using the K-epsilon model." *AIAA journal* 34, no. 2 (1996): 309-316. https://doi.org/10.2514/3.13065
[50] Kurbatskii, Konstantin. "Numerical simulation of three-dimensional jet screech tones using a general purpose finite-volume CFD code." In *49th AIAA Aerospace Sciences Meeting including the New Horizons Forum and Aerospace Exposition*, p. 1085. 2011. https://doi.org/10.2514/6.2011-1085
[51] Kurbatskii, Konstantin. "Scale-resolving simulation of an unsteady turbulent flow and acoustic field of a screeching supersonic jet." In *18th AIAA/CEAS Aeroacoustics Conference (33rd AIAA Aeroacoustics Conference)*, p. 2289. 2012. https://doi.org/10.2514/6.2012-2289
[52] Ramakrishnan, Ramani, Sergio Raimondo, Anant Grewal, and Gary Elfstrom. "Screech suppression of supersonic jet noise." *Canadian Acoustics* 37, no. 3 (2009): 86-87.
[53] Munday, David, Ephraim Gutmark, Junhui Liu, and K. Kailasanath. "Flow structure of supersonic jets from conical CD nozzles." In *39th AIAA fluid dynamics conference*, p. 4005. 2009. https://doi.org/10.2514/6.2009-4005
[54] Ye, Chuang-Chao, Peng-Jun-Yi Zhang, Zhen-Hua Wan, De-Jun Sun, and Xi-Yun Lu. "Numerical investigation of the bevelled effects on shock structure and screech noise in planar supersonic jets." *Physics of Fluids* 32, no. 8 (2020). https://doi.org/10.1063/5.0013263
[55] Li, Hu, Yong Luo, and Shuhai Zhang. "Assessment of upwind/symmetric WENO schemes for direct numerical simulation of screech tone in supersonic jet." *Journal of Scientific Computing* 87, no. 1 (2021): 3. https://doi.org/10.1007/s10915-020-01407-6
[56] Kumar, Bholu, and Shantanu Srivastava. "Modelling 2-D supersonic jet from a convergent-divergent nozzle using k-ε realizable turbulence model." In *Journal of Physics: Conference Series*, vol. 1240, no. 1, p. 012019. IOP Publishing, 2019. https://doi.org/10.1088/1742-6596/1240/1/012019
[57] Testa, Claudio. "Acoustic formulations for aeronautical and naval rotorcraft noise prediction based on the Ffowcs Williams and Hawkings equation." (2008).
[58] Lloyd, T. P., D. Rijpkema, and E. Van Wijngaarden. "Implementing the Ffowcs Williams-Hawkings acoustic analogy into a viscous CFD solver." In *17th Numerical Towing Tank Symposium (NuTTS)*. 2014.
[59] Cianferra, Marta, and Vincenzo Armenio. "Scaling properties of the Ffowcs-Williams and Hawkings equation for complex acoustic source close to a free surface." *Journal of Fluid Mechanics* 927 (2021): A2. https://doi.org/10.1017/jfm.2021.723
[60] Norum, T. D. "Screech suppression in supersonic jets." *Aiaa Journal* 21, no. 2 (1983): 235-240. https://doi.org/10.2514/3.8059
[61] Ponton, M. K., and J. M. Seiner. "The effects of nozzle exit lip thickness on plume resonance." *Journal of Sound and Vibration* 154, no. 3 (1992): 531-549. https://doi.org/10.1016/0022-460X(92)90784-U
[62] Pack, DC0040. "A note on Prandtl's formula for the wave-length of a supersonic gas jet." *The Quarterly Journal of Mechanics and Applied Mathematics* 3, no. 2 (1950): 173-181. https://doi.org/10.1093/qjmam/3.2.173